Progress In Electromagnetics Research C, Vol. 72, 1–13, 2017

A Novel Cavity Backed Monopole Antenna with UWB Unidirectional Radiation

Arezou Edalati*, Wenyi Shao, Todd McCollough, and William McCollough

Abstract—A novel compact unidirectional UWB antenna is presented in this paper. First a novel planar omnidirectional UWB antenna with CPW-feed is designed. The antenna is composed of a half-elliptical disc with a small ground plane. A slot is inserted on the patch as a novel technique to improve the gain bandwidth of the antenna at higher frequencies. The omnidirectional antenna shows UWB matching and gain bandwidth of 2 GHz to 6.5 GHz. Furthermore, to make the radiation pattern of the omnidirectional antenna unidirectional, a rectangular shape metallic reflector without bottom wall is used on the backside of the antenna. The unidirectional antenna with a total dimension of $0.52\lambda_m \times 0.33\lambda_m \times 0.18\lambda_m$ (λ_m wavelength of the minimum operating frequency) has a matching bandwidth of 1.5 GHz to 7.7 GHz with a gain of 5 dBi to 10.2 dBi over 1.7 GHz to 6.5 GHz, and flat group delays of less than 1 nsec. To validate the proposed design, the antenna is fabricated, and measured results are compared with simulations.

1. INTRODUCTION

Ultra-WideBand (UWB) systems have attracted attention for many reasons including their high data rate, low power consumption, and low cost of the RF system front-end [1–3]. These characteristics make UWB systems attractive for many applications such as high data rate communications systems [4, 5], ground penetration radars (GPR) [6, 7], through-wall imaging [8, 9], and biomedical microwave imaging [10, 11]. The main components of UWB systems are UWB antennas. UWB antennas with an omnidirectional radiation pattern are widely used in wireless communication systems [12, 13]; however, for high data rate point-to-point communications, as well as imaging and radar applications, UWB antennas with a unidirectional radiation pattern are preferable so undesirable dissipation of power is minimized.

Vivaldi antennas [14, 15] and double-ridged horn antennas [16, 17] are widely-used UWB directional antennas but have characteristics that limit their applications at low frequencies. Vivaldi antennas require at least a few wavelengths to achieve UWB matching and gain, and double-ridged horn antennas are very bulky. Log-spiral antennas are known for frequency independent bandwidth but are very dispersive, which makes them unsuitable for transmission and reception of short pulses as required in imaging and GPR applications [18]. A drawback of other UWB directional antennas, including resistively loaded V-dipole [19, 20] and coupled sectorial loop antennas [21, 22], is high coupling between adjacent elements, due to their open structures, if they are used in an array configuration. Electromagnetic absorbers between elements can be used to reduce coupling, but this reduces antenna efficiency. A slot-loaded folded dipole antenna with unidirectional radiation is proposed in [23], although this antenna is compact; the bandwidth is only 57%.

Another technique to design a unidirectional UWB antenna is to use a metallic reflector on the backside of an omnidirectional UWB antenna. Bow-tie antennas and wideband dipoles have been used

Received 16 December 2016, Accepted 8 February 2017, Scheduled 27 February 2017
* Corresponding author: Arezou Edalati (aedalati@celadon-inc.com).
The authors are with the Ellumen Inc., 1401 Wilson Blvd, Suite 1200, Arlington, VA 22209, USA.

widely as UWB omnidirectional antennas and backed by a metallic reflector to achieve a unidirectional radiation [24–28]. In [24] and [25] the achieved bandwidth is only 23% and 90% respectively, thus limiting their applications and effectiveness. In [26–28], although UWB matching bandwidth is achieved using a cavity-backed reflector, a balun perpendicular to the antenna plane has to be used for the transition from the microstrip to the stripline feeding, which makes the design and fabrication complicated. Recently, UWB monopole antennas have been used, instead of bow-tie or wideband dipole, to mitigate the drawback of using a balun [29, 30]. However, in [29] the antenna gain has some nulls across the entire UWB frequency, so the antenna performance is not uniform and stable in the entire operating frequency. In addition,using the pyramidal metallic reflector makes the antenna fabrication and implementation difficult as it is not a planar structure. In [30], a monopole UWB antenna is used with a flat metallic plate as a reflector to make the radiation pattern of the antenna directive, but the gain bandwidth of this antenna is only 67% which does not cover the entire UWB frequency range. Furthermore, as the metallic plate is an open structure, this design is not suitable for array configurations due to high coupling between adjacent elements.

To the best of our knowledge, there are few studies or designs of compact directive UWB antennas based on monopole radiator. To overcome the drawbacks of previous designs, we present a novel unidirectional UWB antenna based on a monopole radiator backed with a compact rectangular metallic reflector. First, we design a novel omnidirectional UWB single-sided monopole antenna with CPW-feed that operates from 2 GHz to 6.5 GHz. This frequency range is appropriate for using this antenna in our medical microwave imaging system which operates at a lower frequency band compared to FCC authorized unlicensed UWB range. We also propose a novel technique — the insertion of a slot on the patch — to improve the gain bandwidth of the omnidirectional antenna at higher frequencies; furthermore, we design a compact rectangular metallic reflector on the backside of the omnidirectional antenna to make the radiation pattern unidirectional. By removing the bottom wall of the reflector, we also show antenna gain is improved in the middle of the frequency band. Extensive full-wave simulations, parametric studies, and optimizations are performed on the antenna designed in CST MWS 2016. The advantages of the proposed antenna compared to previous published works are, this antenna is compact with a total dimension of $0.52\lambda_m \times 0.33\lambda_m \times 0.18\lambda_m$ (λ_m is the wavelength of the minimum operating frequency) which is smaller than antennas proposed in [24–30], and it has UWB matching of 1.5 GHz to 7.7 GHz (BW = 134%), gain of 5 dBi to 10.2 dBi from 1.7 GHz to 6.5 GHz (BW = 117%), and flat group delays of less than 1 nsec. As the radiating source is a planar and single-sided antenna, using the Printed Circuit Board (PCB) technology the antenna fabrication is uncomplicated. Moreover, by using a monopole antenna as the radiating source, the design and implementation are very simple as there is no need to use a balun for antenna feeding, unlike designs presented in [24–28]. In addition, as the metallic reflector is a rectangular, flat structure, it is more easily integrated with other technology platforms compared to a parabolic or pyramidal reflector, and having metallic walls on both sides of the omnidirectional antenna makes the directive antenna suitable for any array configurations.

Subsequent sections address the following: In Section 2, we present the design of the novel omnidirectional UWB antenna with parametric studies. Section 3 describes the design of the unidirectional antenna with metallic reflector and presents parametric studies. Measured results of the fabricated unidirectional antenna are presented in Section 4. Finally, concluding remarks are offered in Section 5.

2. PLANAR OMNIDIRECTIONAL UWB ANTENNA

The design of a novel compact and planar UWB omnidirectional antenna with CPW-feed is presented. The radiating element is a half-elliptical disc which is cut from both sides, with an arc on the top. The antenna has a CPW-feed with feed line width of $W_{feed} = 1.4$ mm and $gap_{feed} = 0.25$ mm, and small ground planes on both sides. The substrate is FR-4 with $er = 4.3$, loss tangent of 0.025, and thickness of $h_{sub} = 1.58$ mm. A rectangular slot with elliptical arcs is inserted on the half-elliptical radiator to enhance the antenna gain at higher frequencies. The antenna schematic is shown in Fig. 1 and the final dimensions are presented in Table 1. The radius of the three elliptical curves in the x and y directions are presented with $X_{r\text{-}ellip}$ and $Y_{r\text{-}ellip}$ variables.

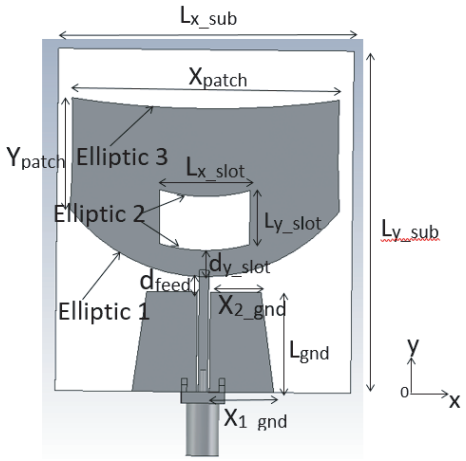

Figure 1. Omnidirectional UWB antenna schematic.

Table 1. Omnidirectional UWB antenna dimensions (mm).

$\mathbf{L}_{x\_sub}$	$\mathbf{L}_{y\_sub}$	$\mathbf{X}_{patch}$	$\mathbf{Y}_{patch}$	$\mathbf{X}_{1\_gnd}$	$\mathbf{X}_{2\_gnd}$
43.19	50.13	39.1	16.31	9.4	7.4
$\mathbf{L}_{gnd}$	$\mathbf{d}_{feed}$	$\mathbf{W}_{feed}$	$\mathbf{gap}_{feed}$	$\mathbf{h}_{sub}$	$\mathbf{d}_{y\_slot}$
14.44	2.22	1.4	0.25	1.58	3.86
$\mathbf{L}_{y\_slot}$	$\mathbf{L}_{x\_slot}$	$\mathbf{X}_{r\_ellip1,2}$	$\mathbf{Y}_{r\_ellip1,2}$	$\mathbf{Y}_{r\_ellip3}$	$\mathbf{X}_{r\_ellip3}$
7.9	13.2	26.62	29.75	7.97	34.24

2.1. Effect of Design Parameters on Antenna Performance

In this section, the effect of important design parameters on omnidirectional UWB antenna radiation performance is presented. One parameter defining the UWB antenna dimensions is allowed to vary while the others are fixed with the dimensions presented in Table 1. The distance between the ground plane and the elliptical radiator, d_{feed}, can be tuned to improve the antenna matching as shown in Fig. 2(a). When the patch radiator is too close to the ground planes, the bandwidth is narrower and the S_{11} becomes higher at the middle of the band. By increasing this distance to a limited extent, the matching bandwidth becomes wider and S_{11} improves. The best S_{11} is achieved with $d_{feed} = 2.22$ mm. The size of the ground plane also affects antenna performances. As shown in Fig. 2(b) and Fig. 2(c), by decreasing the ground plane dimensions the antenna matching and gain are improved respectively; however, if the ground plane is too small the S_{11} and gain are deteriorated.

To improve the antenna radiation performance at higher frequencies and increase the gain bandwidth of the antenna, a rectangular slot with elliptical arcs at the top and bottom, is inserted on the radiating element. By tuning the slot dimensions and position, the current distribution on the radiating element is modified at higher frequencies so it creates uniform field distributions. Therefore, the antenna radiates at boresight and the antenna radiation performance is enhanced as presented in Fig. 3.

The 2D radiation patterns of the omnidirectional antenna in the xz- and yz-planes are presented in Fig. 4 at different frequencies. As shown, the antenna has an omnidirectional radiation pattern over the entire frequency band of operation.

Figures 5(a) and (b) show the effect of the slot length ($L_{x\text{-}slot}$), and the distance between the slot and feed point ($d_{y\text{-}slot}$) respectively, on the antenna gain. By changing these two variables, the antenna gain can be enhanced significantly at higher frequencies while there is no effect on antenna gain at lower frequencies. This is because the slot does not change the current distribution on the patch antenna at lower frequency as it is small compared to the wavelength at lower frequencies. The effect of these

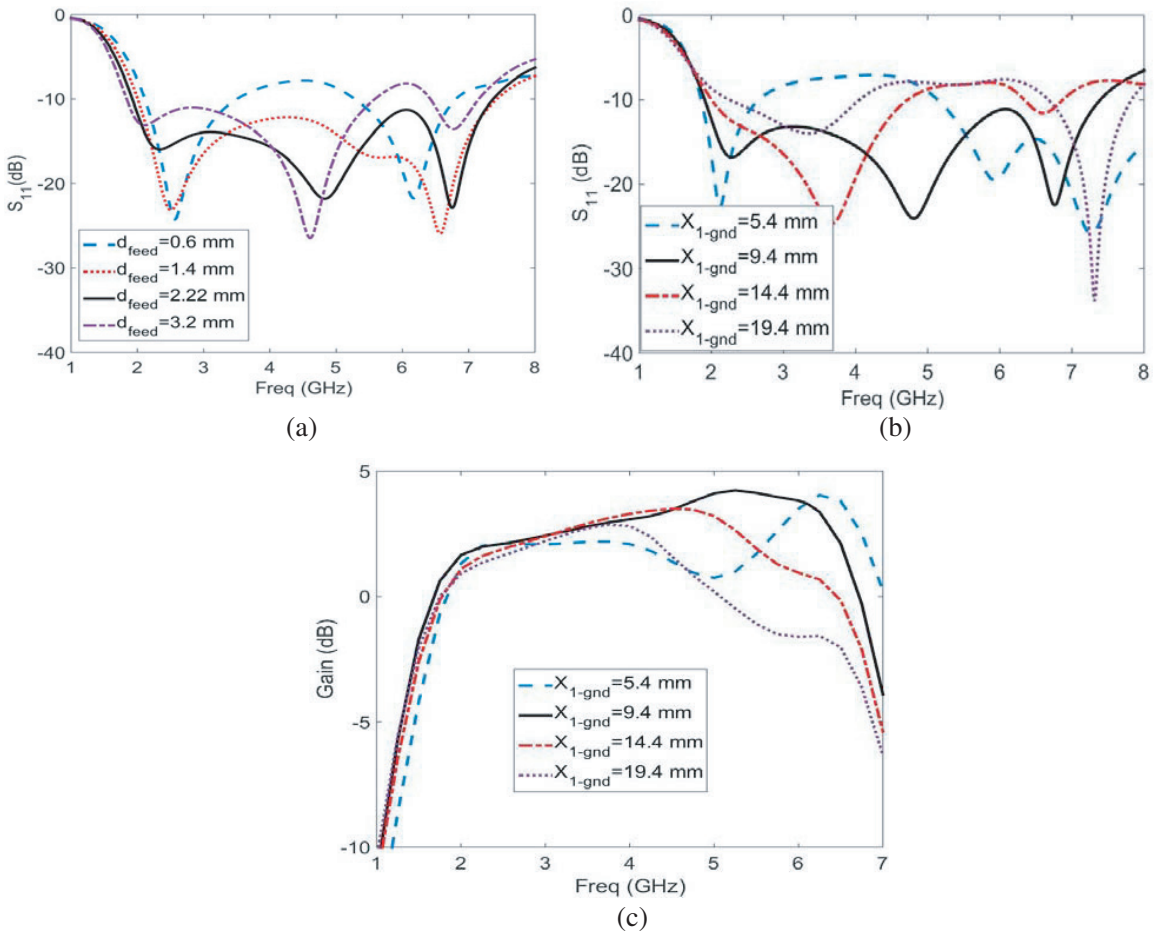

Figure 2. (a) Effect of the distance between the ground plane and the elliptical radiator d_{feed} on antenna matching, (b) effect of the size of the ground plane on the antenna matching when $X_{2\text{-}gnd} = X_{1\text{-}gnd}$-2, (c) effect of the size of the ground on the antenna gain when $X_{2\text{-}gnd} = X_{1\text{-}gnd}$-2.

two design parameters on antenna matching is also shown in Figs. 5(c) and (d). The antenna matching can be modified by changing these two parameters, but the effect is less significant when compared to the antenna gain at higher frequencies, because the slot dimensions have a minor effect on the input impedance of the antenna. The antenna gain and matching is best when using $L_{x\text{-}slot} = 13.2\,\text{mm}$ and $d_{y\text{-}slot} = 3.86\,\text{mm}$.

The proposed planar omnidirectional antenna operates from 2 GHz to 6.5 GHz with gain bandwidth and matching of over 100% and a compact size of $0.33\lambda_m \times 0.28\lambda_m \times 0.01\lambda_m$ which can be used in wireless communication systems.

3. UNIDIRECTIONAL UWB ANTENNA

To make the planar UWB antenna suitable for imaging and radar applications, the antenna should be unidirectional. In addition, the impulse response of the antenna should present a low dispersion characteristic over the frequency band of operation. To make the radiation pattern of the omnidirectional antenna directive, a compact rectangular metallic reflector is placed at the back of the omnidirectional antenna (Section 2) to direct the radiated energy forward, as shown in Fig. 6, with dimensions presented in Table 2. As shown in Fig. 6, the proposed metallic reflector does not have a bottom wall. As discussed in this section, by removing the bottom wall of the reflector the antenna group delays and gain in the middle of the frequency band are improved. In addition, without the bottom wall of the reflector, it is easier to connect the antenna port to a cable.

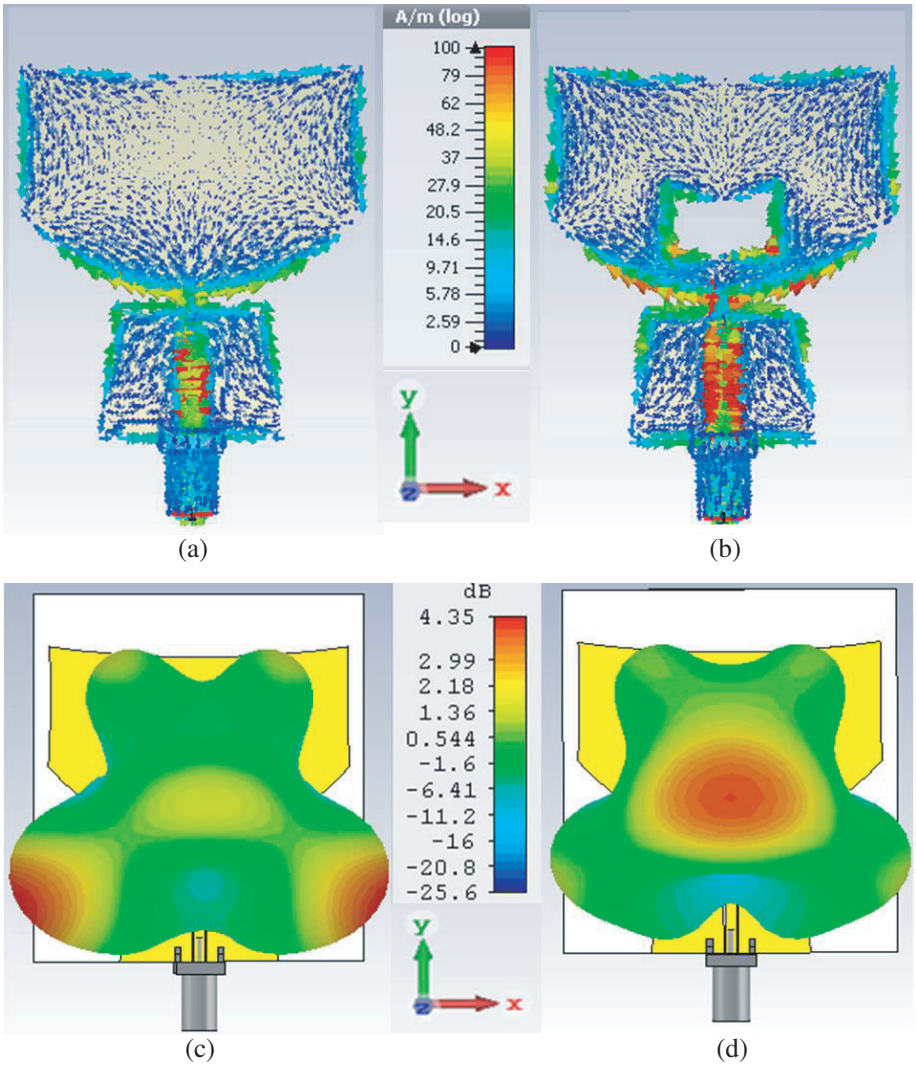

Figure 3. Effect of the rectangular slot on the antenna current distribution [(a) without slot, (b) with slot], antenna radiation pattern [(c) without slot, (d) with slot] at 6 GHz.

Table 2. Dimension of the metallic reflector (mm).

$\mathbf{L}_{x\text{-}reflector}$	$\mathbf{Y}_{t\text{-}reflector}$	$\mathbf{Y}_{b\text{-}reflector}$	$\mathbf{h}_{reflector}$	$\mathbf{d}_{reflector}$
105	51.6	16.25	16	20

3.1. Effect of the Design Parameters of Metallic Reflector on Antenna Performance

In this section, the effect of design parameters of the metallic reflector on the radiation performance of the unidirectional UWB antenna is presented. In each figure, one parameter is varied while the others are fixed with values presented in Table 2. The dimension of the omnidirectional monopole antenna is as presented in Table 1. The main parameter for designing an effective reflector is the distance between the main radiator and the back wall of the metallic reflector, $d_{reflector}$. Figs. 7(a) and (b) present the effect of this parameter on antenna matching and gain respectively. By tuning $d_{reflector}$, optimum matching is achieved. When the monopole antenna is too close to the back wall of the reflector, the matching at lower frequency is reduced. By increasing this distance, the matching at low frequencies is improved to the optimal value. Increasing this distance further deteriorates the matching at higher

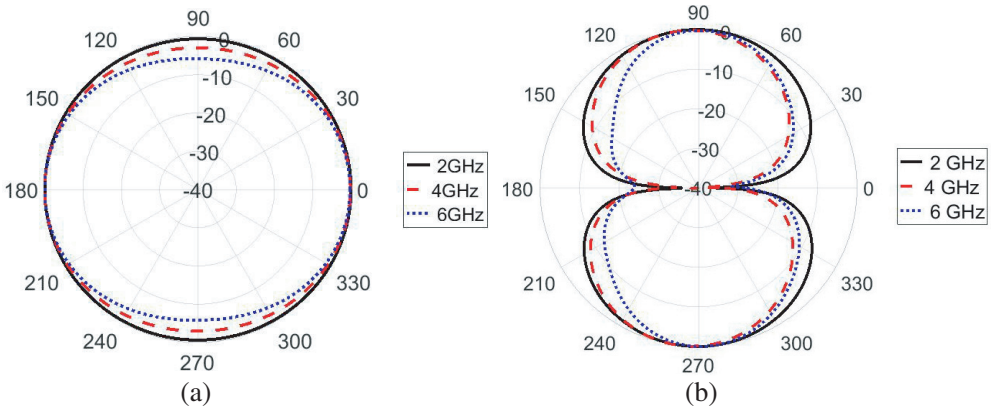

Figure 4. Normalized radiation pattern of the omnidirectional planar antenna, (a) xz-plane, (b) yz-plane.

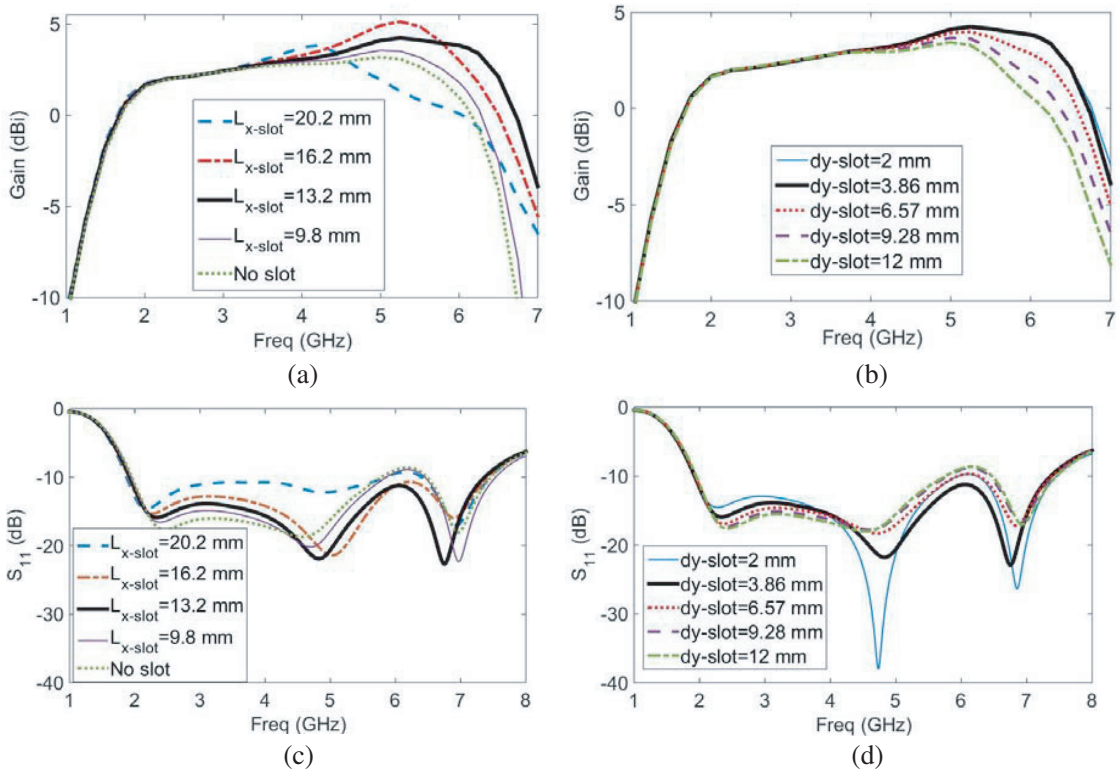

Figure 5. Effect of the length of the slot and distance between slot and feeding point on antenna gain and matching: (a), (b) effect of $L_{x\text{-}slot}$, and $d_{y\text{-}slot}$, on antenna gain, (c), (d) effect of $L_{x\text{-}slot}$, and $d_{y\text{-}slot}$, on antenna matching.

frequencies. In addition, by tuning $d_{reflector}$, the constructive interference between reflected rays from the metallic reflector and direct rays from the omnidirectional antenna is modified which enhances the antenna radiation at boresight, and antenna gain. With $d_{reflector} = 20\,\text{mm}$, UWB matching is achieved while the widest gain bandwidth is reached. The length of the reflector, $L_{x\text{-}reflector}$, can also be tuned to improve antenna matching as presented in Fig. 8(a). The wider reflector length shifts the minimum operation frequency to a lower band, because the lowest operation frequency of the reflector antenna is determined by this length as well as the lowest frequency of the monopole antenna; however, increasing the reflector length deteriorates matching at the higher frequencies. Based on parametric studies and

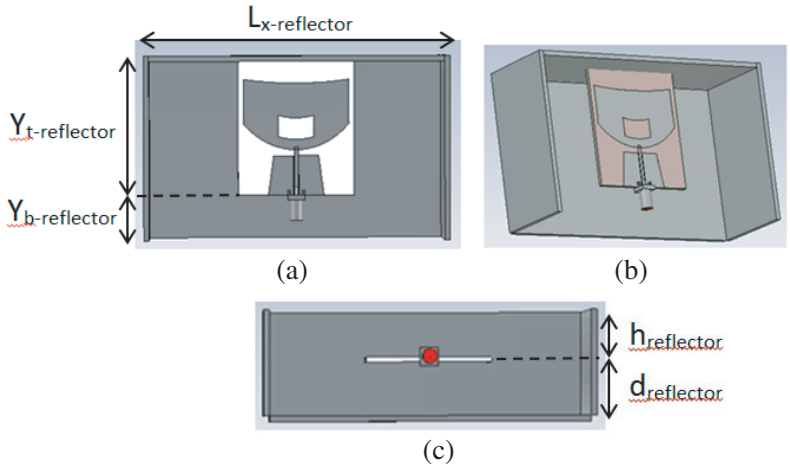

Figure 6. Unidirectional UWB antenna schematic: (a) front view, (b) 3D view, (c) bottom view.

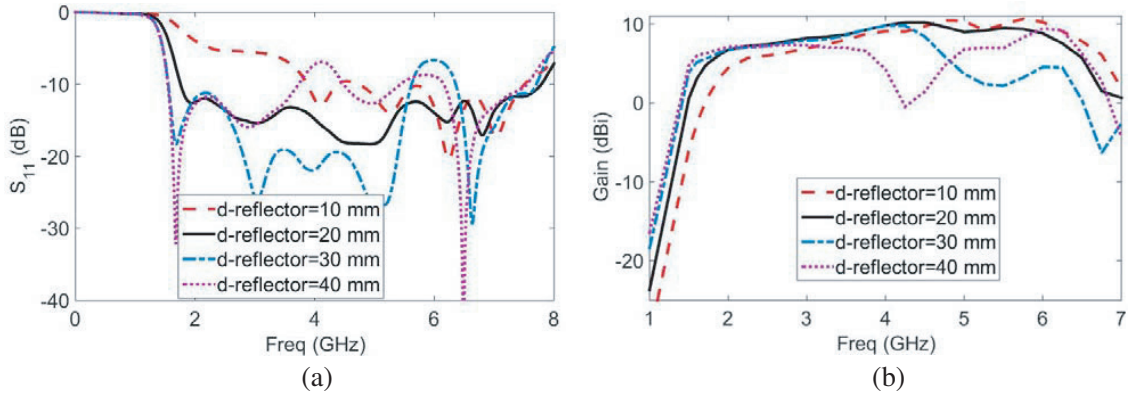

Figure 7. Effect of the distance between the antenna and the metallic reflector back wall, $d_{reflector}$, on (a) antenna matching, (b) antenna gain.

optimization, with $L_{x\text{-}reflector} = 105\,\text{mm}$ a good matching can be achieved. Fig. 8(b) shows the effect of the distance between the antenna feed-point and the top wall of the reflector on antenna matching. By increasing $Y_{t\text{-}reflector}$, the antenna matching worsens, especially in the lower band. The best S_{11} is achieved with $Y_{t\text{-}reflector} = 51.6\,\text{mm}$, when the substrate touches the top wall of the reflector.

Removing the bottom wall of the reflector not only facilitates connecting the antenna to the cable and measurement setup, but also improves antenna group delay. Flat group delays ensure low dispersion of the received signal. By changing the width of the bottom wall ($L_{z\text{-}reflector}$), S_{11} group delay is modified and best when there is no metallic bottom wall as presented in Fig. 9(a). Removing the bottom wall also enhances the antenna gain at the middle of the frequency band as shown in Fig. 9(b).

The final antenna design has $S_{11} < -10\,\text{dB}$ from 1.5 GHz to 7.7 GHz (BW = 134%), and gain of 5 dBi to 10.2 dBi from 1.7 GHz to 6.5 GHz (BW = 117%) with a flat group delay. In addition, compared to prior arts, the proposed antenna is compact with total dimension of $0.52\lambda_m \times 0.33\lambda_m \times 0.18\lambda_m$. Table 3 compares the dimensions of the proposed antenna to selected prior designs to show the compactness of the present design.

The time domain characteristic of the antenna is also calculated using the Fidelity Factor (FF) which identifies the similarity between two signals. The FF value is between 0 to 1, and 1 indicates both signals are identical. The FF is defined as the maximum magnitude of the cross correlation between

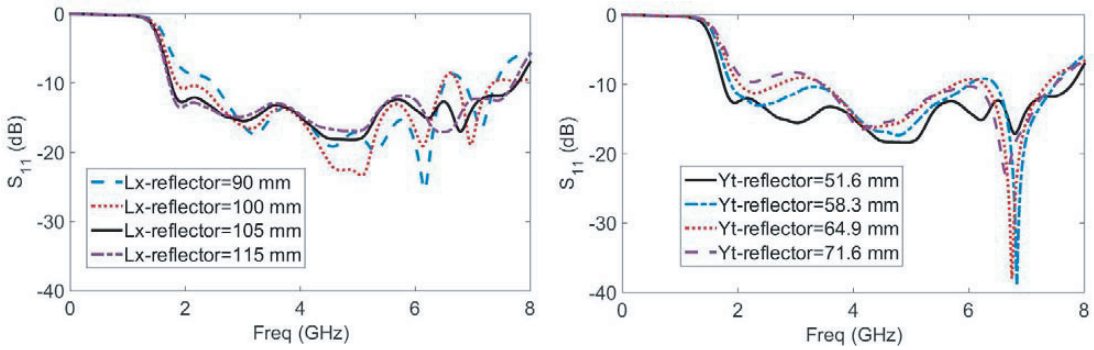

Figure 8. Effect of (a) the length of the metallic reflector, $L_{x\text{-}reflector}$, (b) the distance between the antenna feed-point to the top wall of the reflector, $Y_{t\text{-}reflector}$, on antenna matching.

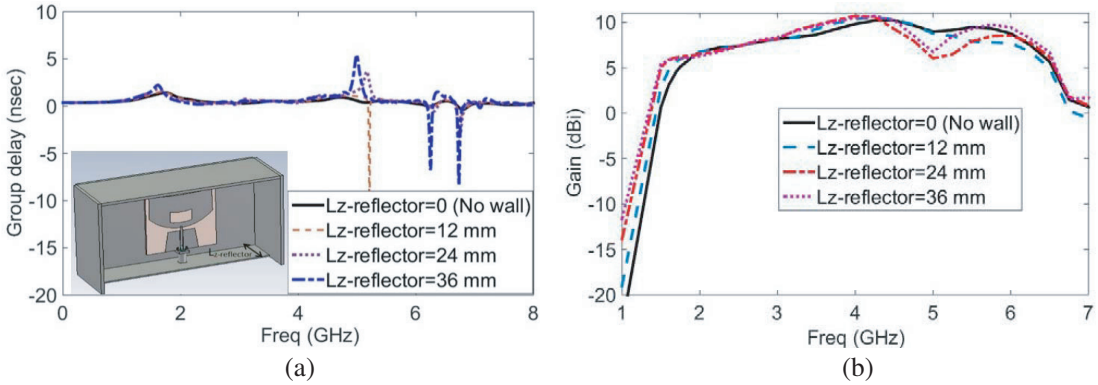

Figure 9. Effect of the width of the bottom wall of the cavity, $L_{z\text{-}reflector}$, on (a) antenna S_{11} group delay, (b) antenna gain.

Table 3. Comparison of the proposed antenna dimensions to some prior arts (unit λ_m^3).

Ref. [24]	**Ref. [25]**	**Ref. [26]**	**Ref. [27]**
$1.76 \times 1.44 \times 0.1$	$1.56 \times 1.56 \times 0.32$	$0.66 \times 0.66 \times 0.16$	$1.48 \times 1.14 \times 0.28$
Ref. [28]	**Ref. [29]**	**Ref. [30]**	**Proposed design**
$0.73 \times 0.73 \times 0.21$	$1.35 \times 1.35 \times 0.28$	$0.7 \times 0.7 \times 0.16$	$0.52 \times 0.33 \times 0.18$

two signals of $si(t)$ and $st(t)$ where both are normalized by their energy:

$$\mathrm{FF} = \max_{\tau} \left[\frac{\int_{-\infty}^{+\infty} si(t) \cdot st(t-\tau) \cdot dt}{\sqrt{\int_{-\infty}^{+\infty} |si(t)|^2 \cdot dt \int_{-\infty}^{+\infty} |st(t)|^2 \cdot dt}} \right] \tag{1}$$

where τ is the time delay to maximize FF in (1).

A full wave simulation using CST MWS is carried out to calculate the FF of the antenna using the method proposed in [31, 32]. A modulated Gaussian pulse is used as the excitation signal:

$$si(t) = \cos 2\pi f_c (t - 4\pi) e^{-\left(\frac{t-4\tau}{\tau}\right)^2} \tag{2}$$

where $f_c = 4.35\,\mathrm{GHz}$ and $\tau = 87\,\mathrm{ps}$.

The Y-directed E-field on an imaginary probe 250 mm away from the antenna aperture is recorded. The FF between the recorded E-field, and the excitation signal and the first derivative of the excitation signal are calculated and yield fidelities of approximately 0.97 and 0.96 respectively.

4. FABRICATION AND MEASUREMENT RESULTS

To validate the design, the unidirectional UWB antenna from Section 3 is fabricated and the antenna performance is measured and compared with simulations. The omnidirectional planar UWB antenna is fabricated using PCB technique on FR4 substrate with a permittivity of 4.3, loss tang = 0.025 and substrate thickness of 1.58 mm. The metallic reflector is made of brass and the planar antenna is held and fixed inside the reflector using plastic screws at the four corners of the omnidirectional antenna. The fabricated antenna is presented in Fig. 10 using the dimensions from Table 1 and Table 2. The matching of both omnidirectional and unidirectional antennas are measured and compared with simulation results and shown in Fig. 11(a). The measured matching of the omnidirectional antenna agrees well with the simulation result. There is just a slight shift in the lower resonance frequency. In the unidirectional antenna, the difference between simulation and measurement results is slightly greater which indicates inaccuracy in the fabrication of the reflector. Measurement inaccuracy also plays a role in the difference between simulation and measured results. However, the measured S_{11} level of the unidirectional antenna remains less than -6 dB and is acceptable. The -6 dB matching bandwidth is 135% from 1.5 GHz to 7.7 GHz, and the -10 dB matching bandwidth is 100% from 2.5 GHz to 7.7 GHz, for the final prototype. The transmission performance of the antenna in the frequency domain is also measured and compared to simulated results when the antennas are placed face to face and 250 mm apart. As shown in Fig. 11(b), the measured and simulated results of the transmission performance of the antenna are in good agreement.

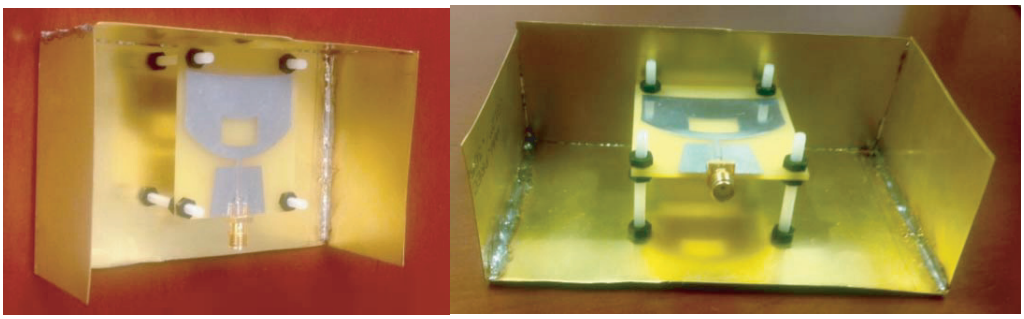

(a) (b)

Figure 10. Fabricated unidirectional UWB antenna.

Another important characteristic of UWB antennas is group delay when they are used in imaging and radar applications. Group delays of the fabricated antennas when they are 250 mm apart at boresight is also measured and compared with simulations in Fig. 11(c). The antenna has S_{11} and S_{21} group delays of less than 1 nsec from 2 GHz to 6.5 GHz.

The time domain characteristic of the proposed antenna is measured when one of the fabricated antennas is connected to an Arbitrary Waveform Generator (AWG70001A) as the transmitter, and the other is connected to an oscilloscope (DPO71604C) as the receiver, when the antennas are face to face and 250 mm apart. The modulated Gaussian pulse is used as the excitation signal. Fig. 12 shows the measured received waveform and compares it to the transmitted signal. For ease of comparison, in Fig. 12, both signals are normalized to their absolute maximum values and shifted to the same time position. There is a small amount of ringing and no widening in the received signal, demonstrating the low dispersion characteristic of the antenna.

The FF of the antenna is also calculated using the method described in [33]. The measured S_{21} is used to calculate the received signal, and the FF identifies the correlation between the received signal and the transmitted signal. A Fidelity Factor of 0.89 is achieved. The reason that the measured FF is less than the FF calculated in the previous section, is the FF here takes into consideration the distortion introduced by both transmitter and receiver antennas by using S_{21}, whereas the simulated FF only considers the distortion introduced by the transmitter antenna. In addition, as the S_{21} was not measured inside an anechoic chamber, the reflection from other objects deteriorates the S_{21} values and hence the FF.

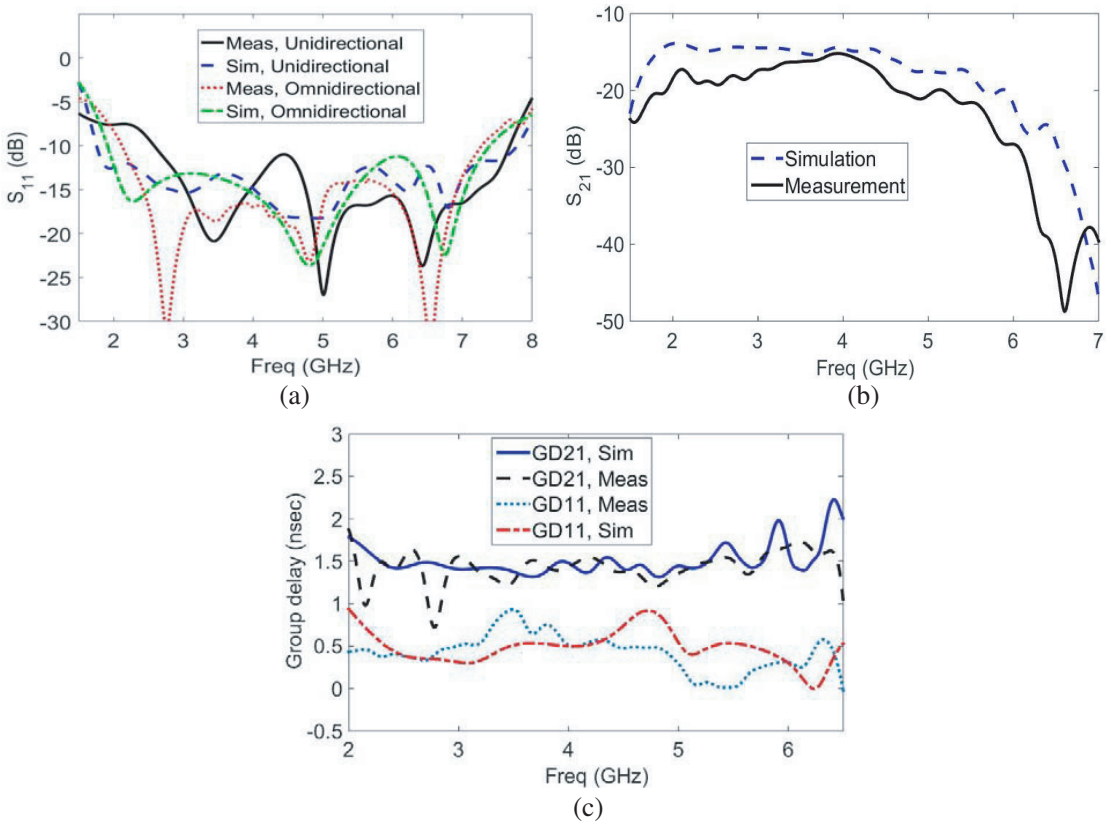

Figure 11. Comparison of the simulated and measured results of (a) antenna S_{11} both unidirectional and omnidirectional, (b) unidirectional antenna S_{21}, (c) unidirectional antenna group delays, when antennas are 250 mm apart (port to port) and placed face to face for transmission and group delay measurements.

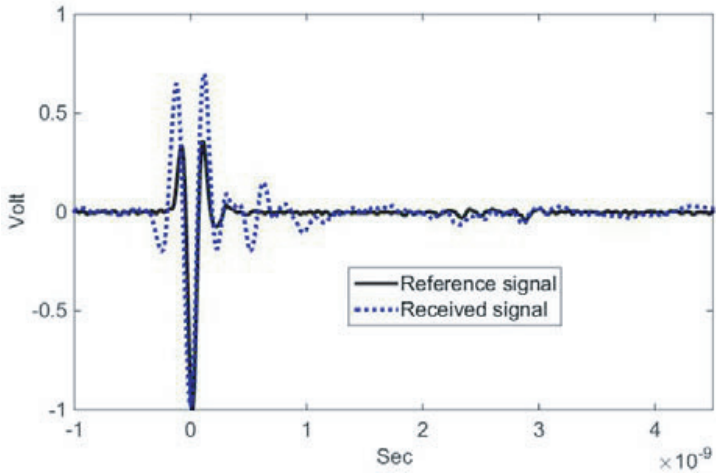

Figure 12. Excitation pulse and received signal in the time domain.

The far-field co-polarization radiation patterns of the antenna at different frequencies (2 GHz, 4 GHz, and 5.5 GHz) are measured and compared with simulated results in Fig. 13. The antenna has a directive radiation pattern. The differences between simulated and measured results in sidelobe levels are due to the inaccuracy in the fabrication of the reflector. To evaluate which parameters cause these

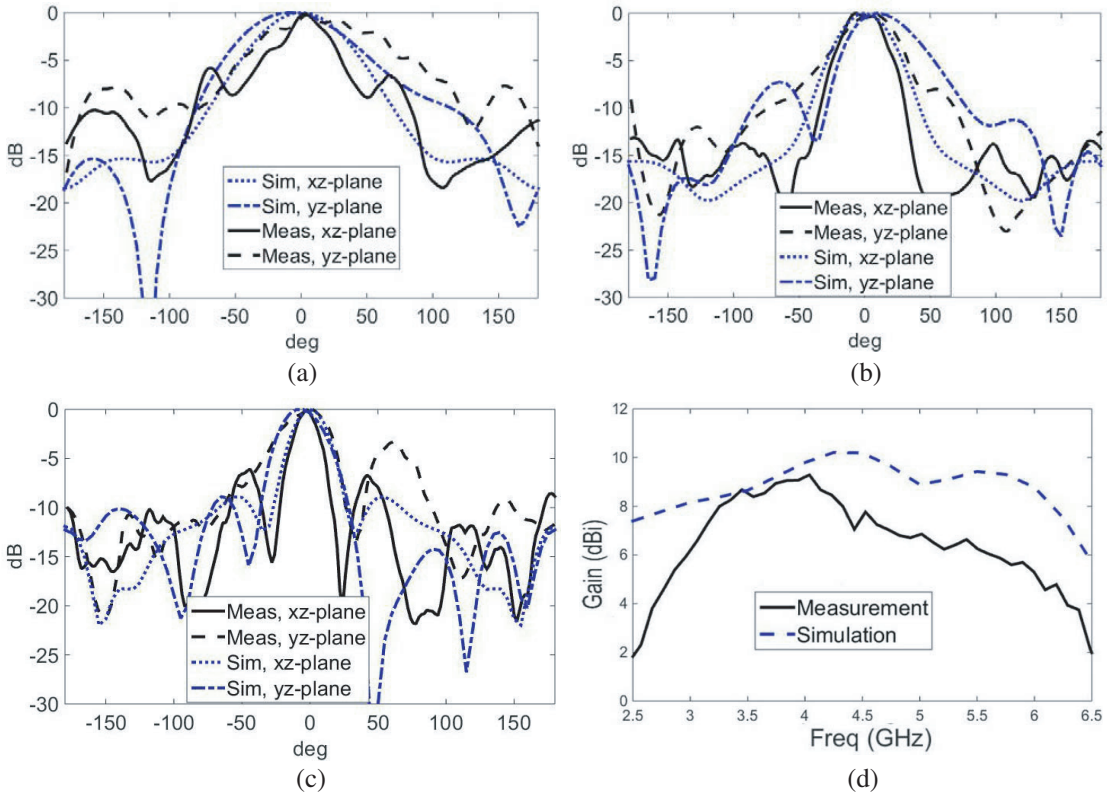

Figure 13. Simulated and measured results for co-polarization radiation patterns of the unidirectional antenna (a) 2 GHz, (b) 4 GHz, (c) 5.5 GHz (d) antenna realized gain.

discrepancies, some parametric studies were run while disturbing the reflector dimensions. The antenna radiation patterns were studied and it was determined that inaccuracy in all the reflector parameters could affect the antenna radiation patterns and sidelobe levels. The antenna realized gain at boresight is also measured and compared with simulated results in Fig. 13(d). The measured realized gain does not follow the simulated results at lower frequencies, likely due to the higher S_{11} at the lower band. Another reason for the discrepancy between simulation and measured gain is that, due to fabrication inaccuracy, the main beam of the antenna is slightly tilted, so the maximum gain is not at boresight, but the measured result presents the realized gain at boresight. A high gain of more than 6 dBi is achieved from roughly 3 GHz to 6 GHz. By fabricating the metallic reflector more accurately and steadily, as well as fixing the omnidirectional planar antenna in an accurate position, the measured radiation patterns and gain of the antenna will be enhanced significantly. It is important to note the discrepancies between simulation and measured results are not due to simulation inaccuracy, as the accuracy of the simulation results was verified by a mesh adaptation technique and a simulation convergence study.

5. CONCLUSIONS

First a novel compact planar omnidirectional UWB antenna is presented. Then, it is shown, by inserting a slot on the patch, that the radiation performance of the antenna at higher frequencies is enhanced. Furthermore, to make the antenna unidirectional, a compact rectangular metallic reflector is designed and used at the backside of the planar UWB antenna. To validate the design, the antenna is fabricated and matching, transmission performance in both time domain and frequency domain, Fidelity Factor, far-field radiation patterns, and gain of the antenna are obtained and compared to simulated results. The simulated and measured results show UWB performance of the antenna with a low dispersion characteristic suitable for radar and imaging applications.

REFERENCES

1. Baumann, C. E., L. Carin, and A. P. Stone, *Ultra-wideband, Short-pulse Electromagnetic 3*, Springer, 2013.
2. Peyrot-Solis, M. A., G. M. Galvan-Tejada, and H. Jardon-Aquilar, "State of art in ultra-wideband antennas," *Proc. 2nd Int. Conf. Electr. and Electron. Eng.*, 101–105, Sep. 2005.
3. Schantz, H. G., *The Art and Science of Ultra-Wideband Antennas*, 2nd edition, Artech House, Boston, MA, 2015.
4. Geng, S., D. Liu, Y. Li, H. Zhuo, W. Rhee, and Z. Wang, "A 13.3 mW 500 Mb/s IR-UWB transceiver with link margin enhancement technique for meter-range communications," *IEEE J. of Solid-State C*, Vol. 50, No. 3, 669-678, Feb. 2015.
5. Heidari, G., *WiMedia UWB: Technology of Choice for Wireless USB and Bluetooth*, 1st edition, Wiley, Hoboken, NJ, USA, 2008.
6. Xu, X., T. Xia, A. Venkatachalam, D. Huston, and M. Asce, "Development of high-speed ultra-wideband ground-penetration radar for rebar detection," *J. of Eng. Mechanic*, Vol. 139, No. 3, 272–285, 2012.
7. Li, L., A. E. Tan, K. Jhamb, and K. Rambabu, "Buried object characterisation using ultra-wideband ground penetrating radar," *IEEE Trans. Microw. Theory Tech.*, Vol. 60, No. 8, 2654–2664, Aug. 2012.
8. Dehmollaian, M. and K. Sarabandi, "Refocusing through building walls using synthetic aperture radar," *IEEE Trans. Geosci. Remote Sens.*, Vol. 46, No. 6, 1589–1599, Jun. 2008.
9. Li, J., Z. Zeng, J. Sun, and F. Liu, "Through-wall detection of human being's movement by UWB radar," *IEEE Geosci. and Remote Sens. Lett.*, Vol. 9, No. 6, 1079–1083, Nov. 2012.
10. Ojaroudi, N., M. Ojaroudi, and N. Ghadimi, "UWB omnidirectional square monopole antenna for use in circular microwave imaging systems," *IEEE Antennas Wireless Propag. Lett.*, Vol. 11, 1350–1353, Nov. 2012.
11. Mobashsher, A. T., A. M. Abbosh, and Y. Wang, "Microwave system to detect traumatic brain injuries using compact unidirectional antenna and wideband transceiver with verification on realistic head phantom," *IEEE Trans. Microw. Theory Tech.*, Vol. 62, No. 9, 1826–1836, Sep. 2014.
12. Edalati, A. and T. A. Denidni, "A compact UWB antenna with dual band-notched characteristics," *Microwave Optical Technology Lett.*, Vol. 52, 1183–1186, 2010.
13. Gautam, A. K., S. Yadav, and B. K. Kanaujia, "A CPW-fed compact UWB microstrip antenna," *IEEE Antennas Wireless Propag. Lett.*, Vol. 12, 151–154, 2013.
14. Bourqui, J., M. Okoniewski, and E. C. Fear, "Balanced antipodal Vivaldi antenna with dielectric director for near-field microwave imaging," *IEEE Trans. Antennas Propag.*, Vol. 58, No. 7, 2318–2326, 2010.
15. Wang, Y., G. Wang, and B. Zong, "Directivity improvement of Vivaldi antenna using double-slot structure," *IEEE Antennas Wireless Propag. Lett.*, Vol. 12, 1380–1383, 2013.
16. Jacob, B., J. W. Odendaal, and J. Joubert, "An improved design for a 1–18 GHz double-ridged guide horn antenna," *IEEE Trans. Antennas Propag.*, Vol. 60, No. 9, 4110–4118, Jul. 2012.
17. Morgan, M. A. and T. A. Boyd, "A 10–100 GHz double-ridged horn antenna and coax launcher," *IEEE Trans. Antennas Propag.*, Vol. 63, No. 8, 3417–3422, Aug. 2015.
18. Daniels, D. J., *Ground Penetrating Radar*, 2nd edition, IET Press, London, UK, 2004.
19. Kim, K. and W. R. Scott, "Design of resistively loaded vee dipole for ultrawide-band ground-penetrating radar applications," *IEEE. Trans. Antennas Propag.*, Vol. 53, No. 8, 2525–2532, Aug. 2005.
20. Yang, H. and K. Kim, "Ultra-wideband impedance matching technique for resistively loaded vee dipole antenna," *IEEE Trans. Antennas Propag.*, Vol. 61, No. 11, 5788–5792, Nov. 2013.
21. Behdad, N. and K. Sarabandi, "A compact antenna for ultrawide-band applications," *IEEE Trans. Antennas Propag.*, Vol. 53, No. 7, 2185–2192, Jul. 2005.

22. Elsherbini, A. and K. Sarabandi, "Directive coupled sectorial loop antenna for ultra-wideband applications," *IEEE Antennas Wireless Propag. Lett.*, Vol. 8, 576–579, 2009.
23. Mobasher, A. T. and A. Abbosh, "Slot-loaded folded dipole antenna with wideband and unidirectional performance for L-band applications," *IEEE Antennas Wireless Propag. Lett.*, Vol. 13, 798–801, 2014.
24. Midrio, M., S. Boscolo, F. Sacchetto, F. M. Pigozzo, and A. D. Capobianco, "Novel ultra-wideband bow-tie antenna with high front-to-back ratio and directivity," *Microwave Optical Technology Lett.*, Vol. 52, No. 5, 1116–1120, 2010.
25. Qu, S. W., J. L. Li, Q. Xue, and C. H. Chan, "Wideband cavity-backed bowtie antenna with pattern improvement," *IEEE Trans. Antennas Propag.*, Vol. 56, No. 12, 3850–3854, Dec. 2008.
26. Qu, S. W., C. H. Chan, and Q. Xue, "Ultra-wideband composite cavity-backed folded sectoral bowtie antenna with stable pattern and high gain," *IEEE Trans. Antennas Propag.*, Vol. 57, No. 8, 2478–2483, Aug. 2009.
27. Ge, L. and K. M. Luk, "A magneto-electric dipole for unidirectional UWB communication," *IEEE Trans. Antennas Propag.*, Vol. 61, No. 11, 5762–5765, Nov. 2013.
28. Tu, Z., D. F. Zhou, G. Q. Zhang, F. Xing, X. Lei, and D. W. Zhang, "A wideband cavity-backed elliptical printed dipole antenna with enhanced radiation patterns," *IEEE Antennas Wireless Propag. Lett.*, Vol. 12, 1610–1613, 2013.
29. Moody, R. A. and S. K. Sharma, "Ultrawide bandwidth (UWB) planar monopole antenna backed by novel pyramidal-shaped cavity providing directional radiation patterns," *IEEE Antennas Wireless Propag. Lett.*, Vol. 10, 1469–1472, 2011.
30. Zhu, F., S. Gao, A. T. S. Ho, T. W. C. Brown, J. Z. Li, and J. D. Xu, "Low-profile directional ultra-wideband antenna for see-through-wall imaging applications," *Progress In Electromagnetic Research*, Vol. 121, 121–139, 2011.
31. Wu, Q., R. Jin, J. Geng, and M. Ding, "Pulse preserving capabilities of printed circular disk monopole antennas with different grounds for the specified signal forms," *IEEE Trans. Antennas propag.*, Vol. 55, No. 10, 2866–2873, 2007.
32. Molaei, A., M. Kaboli, S. A. Mirtaheri, and M. S. Abrishamiyan, "Dielectric lens balanced antipodal Vivaldi antenna with low cross-polarisation for ultra-wideband applications," *IET Microw. Antennas Propag.*, Vol. 8, No. 14, 1137–1142, 2014.
33. Li, X., S. C. Hagness, M. K. Choi, and D. W. van der Weide, "Numerical and experimental investigation of an ultrawideband ridge pyramidal horn antenna with curved launching plane for pulse radiation," *IEEE Antennas Wireless Propag. Lett.*, Vol. 2, 252–269, 2003.